Examining the population of free floating planets

Mohsen Farzone

Lund Observatory
Lund University

2010-EXA44

Degree project of 15 higher education credits
June 2010

Lund Observatory
Box 43
SE-221 00 Lund
Sweden

Examining the population of free floating planets

Mohsen Farzone

July 20, 2010

Supervisors: Melvyn B. Davies, Ross Church

Abstract

Scattered in our galaxy today are planets that have no host star and are only bound to the galaxy. These so called free floating planets are believed to be formed around stars but have later been ejected by passing stars perturbing their orbits, or have undergone close interactions with another planet in a planetary system. This results in one of the planets becoming tightly bound in an often eccentric orbit and the other one ejected. In this project, we simulate the process of stars and their attributes that favours the creation of planets, which through planet-planet interaction processes, populate as free floating planets. The results show that the population of free floaters are much less than expected when compared to the latest observational data. An explanation might be the problem that observations don't distinguish between free floating planets and planets in very wide orbits, or that we simply don't know enough about the parameters involved.

Contents

1 What do we know about exoplanets? 5

2 What is a FFP? 8

3 What is microlensing? 8

4 The project 13
4.1 Stage One . . . 13
4.1.1 Stellar Mass . . . 13
4.1.2 Assigning stellar ages . . . 15
4.1.3 Stellar evolution . . . 15
4.1.4 Stellar metallicities . . . 17
4.1.5 Planet population . . . 17
4.1.6 Planetary mass distribution . . . 18
4.2 The program . . . 19
4.3 Stage Two . . . 20
4.4 Stage Three . . . 22

5 Results 24
5.1 First run . . . 24
5.1.1 Stage One . . . 24
5.1.2 Stage Two & Three . . . 29
5.2 Uncertainties . . . 31
5.2.1 Stellar metallicity . . . 31
5.2.2 Star formation Rate . . . 31
5.2.3 Main sequence lifetime . . . 32
5.2.4 Planet mass distribution . . . 33

6 Discussion 37

7 Acknowledgements 38

1 What do we know about exoplanets?

To this date, a total number of 370[1] planetary candidates have been identified outside our own solar system according to *The Exoplanet Orbit Database* (`exoplanets.org`). These planets are referred to as *extrasolar planets* or *exoplanets*. Many of these lack a similar analog in our own solar system and are usually very extreme, for instance Jupiter-mass planets at orbits closer than Earth around the Sun (1 AU). Looking at how they are placed in a semi-major axis (a) vs. eccentricity (e) plot (Figure 1) one sees a large spread of eccentricities.

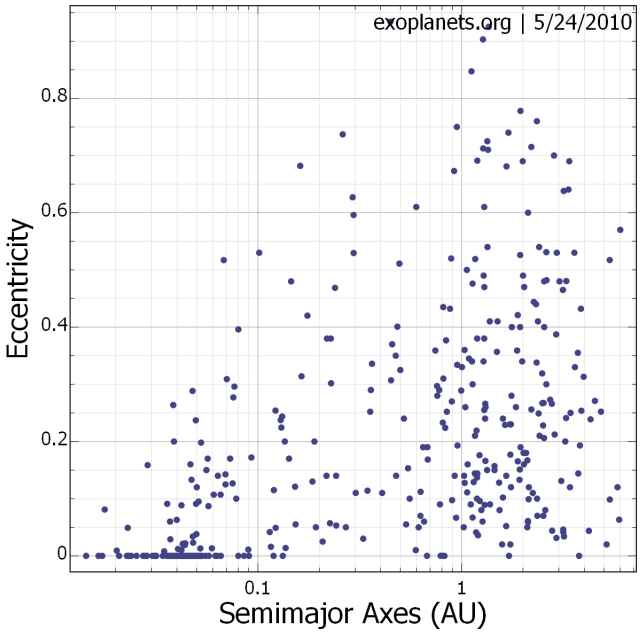

Figure 1: Log semi-major axis vs eccentricity plot of the 370 detected exoplanets from the *The Exoplanet Orbit Database* using all detection methods. There are a large spread of eccentricities for the exoplanets found.

The planets in our own solar system don't have a large spread of eccentricity. Their orbits are of the order 10^{-2} in eccentricity, which means fairly circular. Exceptions are Mercury's orbit at $e \simeq 0.2$ and Pluto at $e \simeq 0.25$ (Beatty & Chaikin, 1990) but Pluto is believed to have a different origin to the major planets of the solar system.

A majority of the points in Figure 2 are from single exoplanet systems,

[1] *The Extrasolar Planets Encyclopaedia* states 461 planetary candidates. The ones used here are from *The Exoplanet Orbit Database* which according to the authors, only includes the most secure and peer-reviewed exoplanet orbital measurements and an upper planetary mass cutoff of 24 Jupiter masses (M_{ju}).

i.e stars with one planet as seen in Table 1.

Systems with	$N_{Systems}$	Fraction of $N_{TotSystems}$
1 planet	277	$\approx 88\%$
2 planets	28	$\approx 8.8\%$
3 planets	8	$\approx 2.5\%$
4 planets	2	$\approx 0.6\%$
5 planets	1	$\approx 0.3\%$

Table 1: Current exoplanet data from The Exoplanet Orbit Database where $N_{TotSystems} = 316$

In addition to the lack of exoplanets similar to those in our own system, an extrasolar system similar to our own has yet to be found (Figure 2).

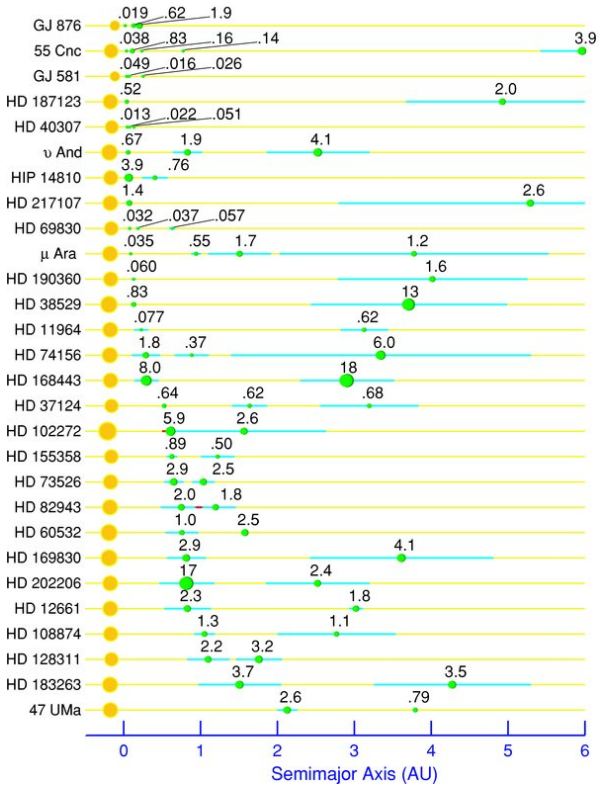

Figure 2: (Wright et al., 2009) Chart of semi-major axis and minimum masses for 28 known multi-planet systems. The diameters depicted for planets are proportional to the cube root of the planetary $M \sin i$. The shortest to longest distance from the host star is shown by a horizontal line intersecting the planet.

One must bear in mind that the method that has been most successful in detecting exoplanets, namely the *radial velocity* or *Doppler method*, hasn't

got a uniform detectability. This method searches for periodic changes in the target star's motion relative the observer which could be induced by an exoplanet orbiting that star. Because of this, heavier planets at tighter orbits are easier to find (larger changes in the relative motion).

If a multi-planet system has crossing orbits, the planets in those orbits may come close to each other and undergo strong *planet-planet interaction* (Figure 3).

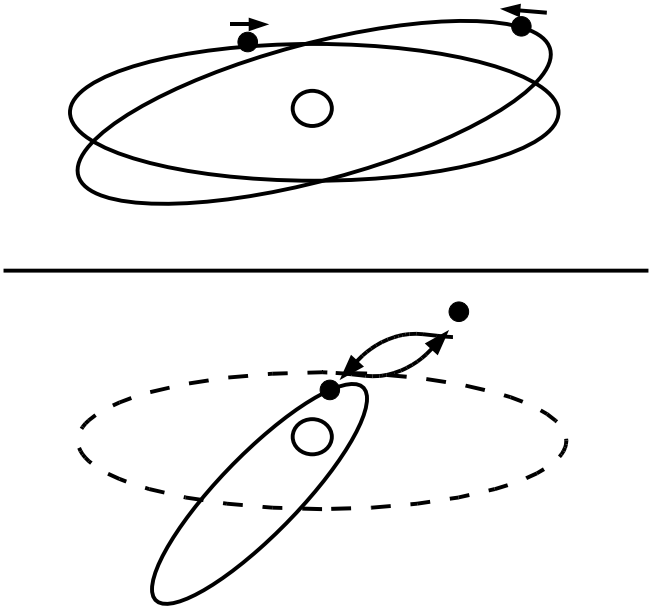

Figure 3: A schematic diagram of a strong planet-planet interaction. The crossing of two planetary orbits (Above) could result in the planets drawing sufficiently near to each other for scattering to occur, leaving one of the planets unbound to the host star and the other one more tightly bound in an eccentric orbit (Bottom).

In the case of two planets in circular orbits, scattering often leaves one of the planets in a more eccentric orbit due to the energy transfer between them and the latter one unbound to the host star (Malmberg & Davies, 2009). Generally, two situations can cause this effect. One is the case of the orbits being perturbed by a passing star, a fly-by. If the orbits after the fly-by are eccentric enough to cross, there might be strong planet-planet interaction. The second case involves the oscillation of eccentricity of two planets much like the interaction between Jupiter and Saturn, which slowly change their eccentricity over the course of many years in a sinusoidal fashion. If the oscillations grow in amplitude, we have a *self-unstable system*. In such a system the orbits might grow to a point at which they cross and again have a chance of strong planet-planet interaction and ejection of planets.

2 What is a FFP?

If an orbiting planet is given enough velocity through the interaction explained earlier and reaches the escape velocity, it has enough energy to escape its host system and become unbound from it. At this moment it's called a *free floating planet* (FFP) and is essentially only bound to the galaxy. Since the gravitational force extends to infinite distances, a free floating planet could also be a planet in a very wide orbit.

To escape the solar system, an object at the distance of 1 AU from the Sun would require $\sim 40\ km/s$. Note that the object's escape velocity doesn't depend on its mass. Our sun is located in the disc of the galaxy, roughly 8.5 kPc from the center. The orbital speed of our Sun in the galaxy is of the order $\sim 200\ km/s$ and thus the escape velocities would be of the same order of magnitude. This means that at the event of planet ejection, the planet would most likely end up in the disc of the galaxy. In other words, the orbits of the FFPs around the galaxy won't have a great height above the galactic plane (and as an additional note, will stay in the near vicinity of it's former host star). Conveniently, in the method of detecting these free floating planets, namely *Gravitational Microlensing*, one looks towards the center of the galaxy that is through the disc, because of the galactic position of the Sun.

3 What is microlensing?

The theory of general relativity predicts that light is affected by gravity. Seen in Figure 4 is a simple illustration of this.

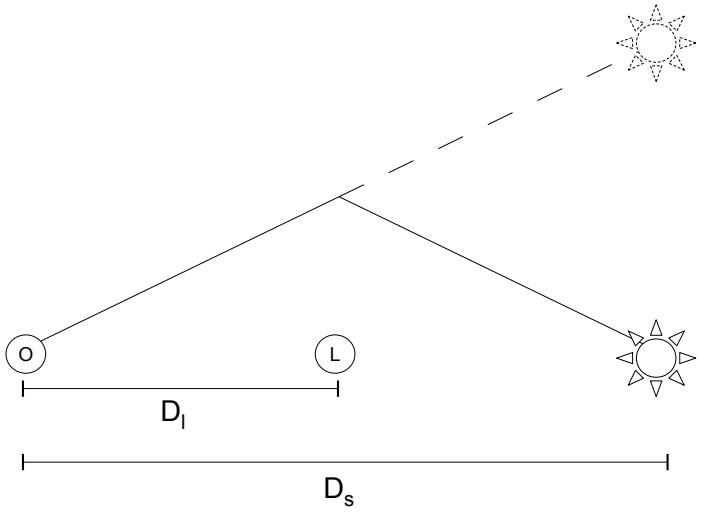

Figure 4: The basics of microlensing. When in alignment, the light from a source star at distance D_s from the observer (O) gets bent due to the gravitational effect of a massive object between the observer and the source, appropriately called a lens (L) at a distance of D_l, and focused on the observer.

Gravitational microlensing is a phenomena based on this and with the use of simple geometry and general relativity, it can be explained from a standpoint of theory (Gaudi, 2010a; Gould, 2001).

Gravitational microlensing (μL) occurs when a foreground massive object (lens) passes close to the line of sight of a distant star (source). The source becomes brighter as the observer, source and lens are aligned in the line of sight and returns to it's regular intensity as they become unaligned again. This whole process is called a *microlensing event* or μL *event*. For an event to occur, would require a very precise alignment which makes it rare. So rare that Einstein (Einstein, 1936) deemed it highly unlikely to happen. To maximise the odds, the microlensing surveys target sources in the center of our galaxy where the stellar density is the highest. The distances to the sources D_s will then be around 8.5 kPc.

A more detailed description of microlensing is seen in Figure 5.

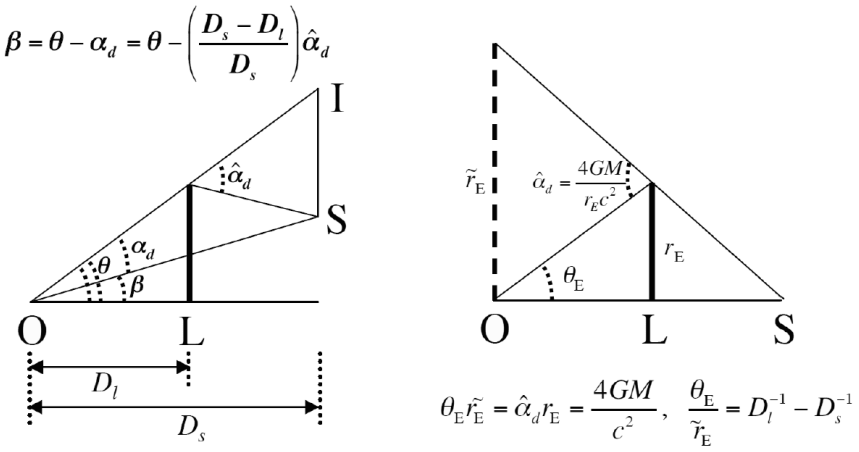

Figure 5: More detailed description of microlensing. The figure to the left describes the general case of an unaligned source (S), lens (L) and observer (O) and the resulting image (I). Whereas they are in alignment in the right figure.

Here the left image depicts the unaligned case which means an unlensed source and the right at full alignment (lensed source). β is a measure of alignment between the source and the observer in the absence of lensing and θ is the angular position of the image of the lensed source.

Light from the source (S) at the distance D_s from the observer (O) gets deflected by a lens (L) by an angle of

$$\hat{\alpha_d} = \frac{4GM}{r_E c^2} \tag{1}$$

for a point mass lens M and impact parameter of r_E. An assumption that the lens has no spatial extent is made which is valid because of large distances between the observer and the lens. In the absence of lensing (left image), the relation between the angular position of the image θ and unlensed source β is given trivially by

$$\beta = \theta - \alpha_d \tag{2}$$

Since the distances involved are great (the order of kPc), using the small angle approximation and simple geometry, one gets $\hat{\alpha_d}(D_s - D_l) = \alpha_d D_s$ and $r_E = D_l\theta$. Combining these with the two above equations:

$$\beta = \theta - \alpha_d = \theta - \left(\frac{D_s - D_l}{D_s}\right)\hat{\alpha_d}$$
$$\beta = \theta - \frac{4GM}{c^2\theta}\frac{D_s - D_l}{D_s D_l}$$

In the case of perfect alignment $\beta = 0 \Rightarrow \theta \equiv \theta_E$

$$\begin{aligned}\theta_E &= \sqrt{\frac{4GM}{c^2}\frac{D_s - D_l}{D_s D_l}} \\ &= \sqrt{\kappa M \cdot \frac{D_s - D_l}{D_s D_l}} \\ \theta_E &= \sqrt{\kappa M \pi_{rel}}\end{aligned}$$

where $\kappa = \frac{4G}{c^2 AU} \simeq 8.14\ mas \cdot M_\odot^{-1} \cdot AU^{-1}$ and π_{rel} is the relative lens-source parallax

$$\pi_{rel} = \frac{1\ AU}{(D_l^{-1} - D_s^{-1})^{-1}} = \frac{1\ AU}{D_{rel}}$$

θ_E is called the *Einstein angle* and when perfectly aligned, the source gets imaged into an "Einstein ring" with a radius of θ_E, the size of which is very small. Using a typical value for D_l somewhere between us and the source and a D_s at 8.5 kPc (center of our galaxy), one gets to an Einstein angle around $\theta_E \simeq 500\ mas$. This corresponds to a physical ring

$$r_E = \theta_E D_l \tag{3}$$

where $r_E \sim AU$. As noted before, the lens, source and observer are in relative motion between each other. The magnification will thus be a function of time and the μL event will have a duration. The duration t_E is the time-scale to cross the angular Einstein ring radius

$$t_E \equiv \frac{\theta_E}{\mu_{rel}} \tag{4}$$

where μ_{rel} is the proper motion of the source relative the lens. Inserting the equation for θ_E yields:

$$t_E = \sqrt{\kappa M \pi_{rel}} \cdot \mu_{rel}^{-1}$$

which can be simplified to only be a function of stellar mass. Using typical values of $\mu_{rel} = 125\ \mu as$ and $\pi_{rel} = 10.5\ mas/yr$

$$t_E \approx 25\ d\ \left(\frac{M}{0.5\ M_\odot}\right)^{1/2} \tag{5}$$

(Gaudi, 2010b)
As one easily can notice, inserting a star with $M = 0.5\ M_\odot$ will yield a $t_E = 25\ d$. A planetary mass of 1 $M_{ju} \approx 0.001\ M_\odot$ will instead produce a t_E of

$$t_E \approx 25\ d\ \left(\frac{0.001\ M_\odot}{0.5\ M_\odot}\right)^{1/2} \approx 1.1\ d \tag{6}$$

Thus the duration of an event caused by a planet will be significantly shorter than one caused by a star simply because of the mass difference between the two. This is emphasised in Figure 6.

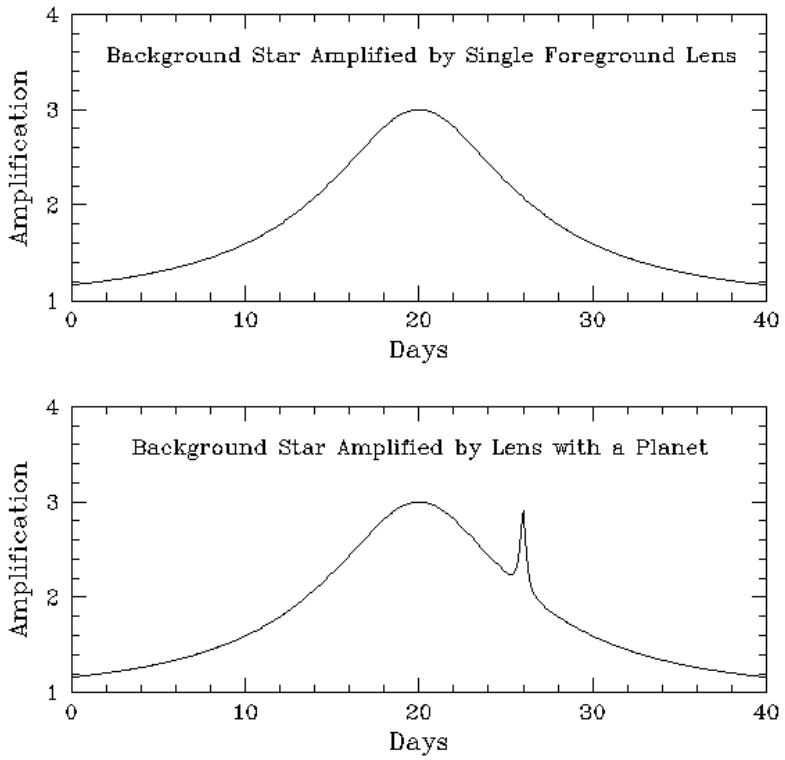

Figure 6: (*Top*) A classical microlensing event of a source star as it is amplified by a passing foreground lens.
(*Bottom*) In this case the lens is instead a binary, a star and a planet. The planet also acts as a lens but will because of the lower mass cause a shorter duration.
(PLANET collab. - `http://planet.iap.fr/planeet.html`)

The top curve is a microlensing event with the lens being a single star and the bottom a star and with a planet. Important aspects to remember with gravitational microlensing is that these curves are taken using light from the source (background) star and NOT the lens, since it's the light from the source that gets amplified and not vice versa. The other one is that this project treats free floating planets and NOT extrasolar systems. However, using Figure 6 one can clearly depict the planet having a smaller duration than the star, which was proven in the equation above. The so far only method of detecting free floating planets is via gravitational microlensing and with a range of sensitivity that spans to the kPc range, few methods can match it and verify the detections even if the planets are fairly luminous, providing this method a large weakness.

4 The project

The main goal of this project was to answer the question:

How many stellar μL-events does one need to see before one expects to see one that is caused by a FFP?

To solve the problem, it was broken down into three stages. Stage one involved the creation of a stellar and a free floating planet population. Stage Two was about determining the relative rate of μL-events and Stage Three determined the probability of an event being registered by a detector, the so called "Detector efficiency". Combining Stage 1–3 would result in the relative rate of registering events caused by FFPs compared to typical lensing stars, which is the main goal of this project.

4.1 Stage One

4.1.1 Stellar Mass

The stellar mass isn't distributed in a trivial way. The *initial mass function* or *IMF* (Kroupa, 2001) is described as a multi-part power law

$$dN = \xi(m)dm \tag{7}$$

$$\xi(m) = k \begin{cases} c_1 \cdot m^{-0.3\pm0.7} & 0.01 \leq m/M_\odot < 0.08 \\ c_2 \cdot m^{-1.8\pm0.5} & 0.08 \leq m/M_\odot < 0.50 \\ c_3 \cdot m^{-2.7\pm0.3} & 0.50 \leq m/M_\odot < 1.00 \\ c_4 \cdot m^{-2.3\pm0.7} & 1.00 \leq m/M_\odot < 120 \end{cases}$$

where k is a normalisation constant. Since we are interested in a relative distribution, namely $\frac{N_\star}{N_{FFP}}$, there is no need of evaluating k. However, there is still the need of connecting the different power-law parts by evaluating c_1 to c_4. Immediately one can see that $c_3 = c_4$ since at $m = 1$:

$$c_3 \cdot m^{-2.7\pm0.3} = c_4 \cdot m^{-2.4\pm0.7}$$

$$\Rightarrow c_3 = c_4 = 1$$

From respect to these, we can derive the other constants

$$\begin{aligned} c_1 &= 0.5^{-0.9} \cdot 0.08^{-1.5} \\ c_2 &= 0.5^{-0.9} \\ c_3 &= 1 \\ c_4 &= 1 \end{aligned}$$

Now connected, the IMF is easier represented in a logarithmic form

$$
\begin{aligned}
y &= \log_{10} m \\
\frac{dy}{dm} &= \frac{1}{m \ln 10} \\
\frac{dN}{dy} &= \frac{dN}{dm} \cdot \frac{dm}{dy} \\
\frac{dN}{d \log_{10} m} &= \frac{dN}{dm} \cdot m \ln 10
\end{aligned}
$$

$$
\Rightarrow \xi(\log_{10} m) = \xi(m) \cdot m \ln 10
$$

Since the conversion to logarithmic form yielded an additional factor m, the power-laws will change. This is shown in the equation below and visualised in Figure 7.

$$
\begin{aligned}
\frac{dN}{dm} &\propto m^{-\alpha} \\
\frac{dN}{d \log m} &\propto m * m^{-\alpha} = m^{1-\alpha}
\end{aligned}
$$

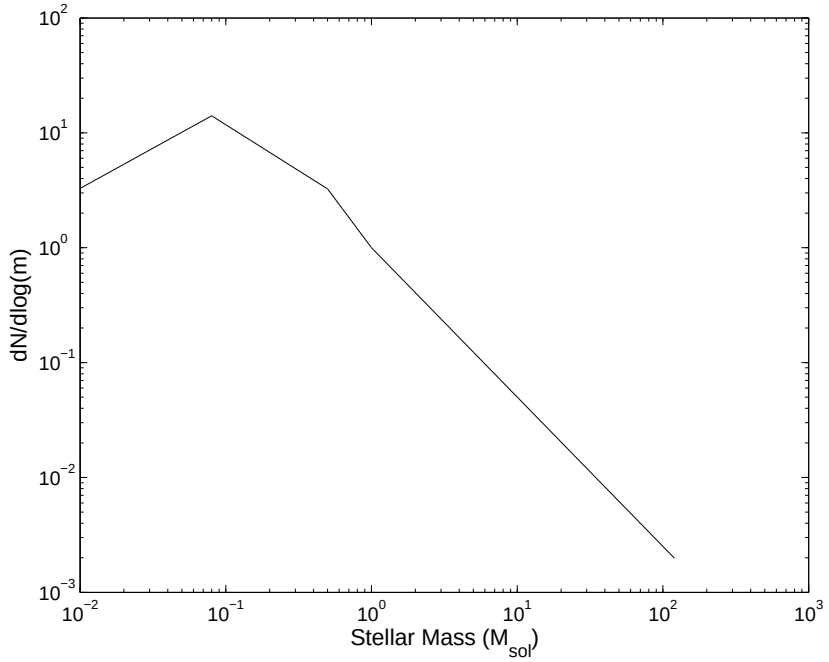

Figure 7: Initial Mass Function (IMF) in a logarithmic form using Kroupa (2001). The function is a 4-part power law, where each part represents a mass range corresponding to a named population (for instance Brown Dwarfs or M-dwarfs etc.). The function has not been normalised for reasons explained in the text.

The different named populations corresponding to the mass ranges where calculated and compared with the ones provided by Kroupa (2001) in order to check for consistency (Table 2).

	Calculated	Kroupa 2001
Brown Dwarf ($0.01 - 0.08\ M_\odot$)	50%	50%
M-Dwarf ($0.08 - 0.5\ M_\odot$)	43 %	44%
K-Dwarf ($0.5 - 1.0\ M_\odot$)	4.2%	4.3%
G - O stars ($1.0 - 120\ M_\odot$)	2.4%	2.5%
$< m >$	0.20 $M_\odot$	0.20 $M_\odot$

Table 2: Comparision of the named populations with their mass ranges given in Kroupa 2001 and the calculated ones using the IMF provided in the same paper

The populations agrees to a high degree. The reason that they differ slightly is probably due to accuracy in the numerical calculation used to acquire the numbers. Using Equation 5, the conversion between event time-scales and masses is easily done, provided the basic assumptions presented with the equation are followed.

4.1.2 Assigning stellar ages

The initial mass function is phrased such a way because it doesn't treat the evolution of stars. The function describes the distribution of masses at the instance of creation ($\tau = 0$). The current distribution of masses (Present-Day Mass Function or PDMF) is an IMF with the aging/evolution of stars, but also the creation of new stars taken into account.
The creation of stars is described by the Star Formation Rate (SFR) and usually has the unit of [mass/time]. When assigning ages to stars, one has to examine the SFR history, i.e the SFR as a function of time. The distribution of stellar ages would follow this. For instance, if there was a sudden peak of star formation at a certain time, a higher percentage of stars would have an age corresponding to when that peak occurred.

A uniform or flat SFR history means a uniform distribution of ages. In other words, in a given interval the odds of a star having a certain age is as probable as having another where maximum stellar age is set to be roughly the Hubble time

$$\tau_{max} = 10^{10}\ Yrs = 10\ Gyrs$$

4.1.3 Stellar evolution

Stars generate energy through nuclear processes and send it out via electromagnetic radiation, resulting in a change in its chemical composition over

time. This is the *Mass-Luminosity relation* that roughly states the following:

$$L \propto m^3$$

The so-called *main sequence* (MS), where our Sun currently is located, is a period when stars produce helium in their cores from nuclear fusion of hydrogen and are in hydrostatic equilibrium. Eventually MS stars will have burnt most of their hydrogen deposits and moved on to other stages. The time that the star spends on the MS depends on how much material there is to burn (mass), but also at the rate at which it's burned. Higher temperature increases the rate of fusion, meaning higher luminosity. Therefore MS lifetime τ_{MS} can simply be expressed in the following way

$$\tau_{MS} \propto \frac{m}{L} \propto m^{-2}$$
$$\tau_{MS} \approx A \cdot m^{-2}$$

In order to fix the relation, the lifetime of the Sun, approximately $\tau_{MS}(1M_\odot) = 10^{10}$ years, was chosen.

$$\tau_{MS}(m) \approx 10^{10} \cdot m^{-2} \; years \tag{8}$$

The equation is visualised in Figure 8.

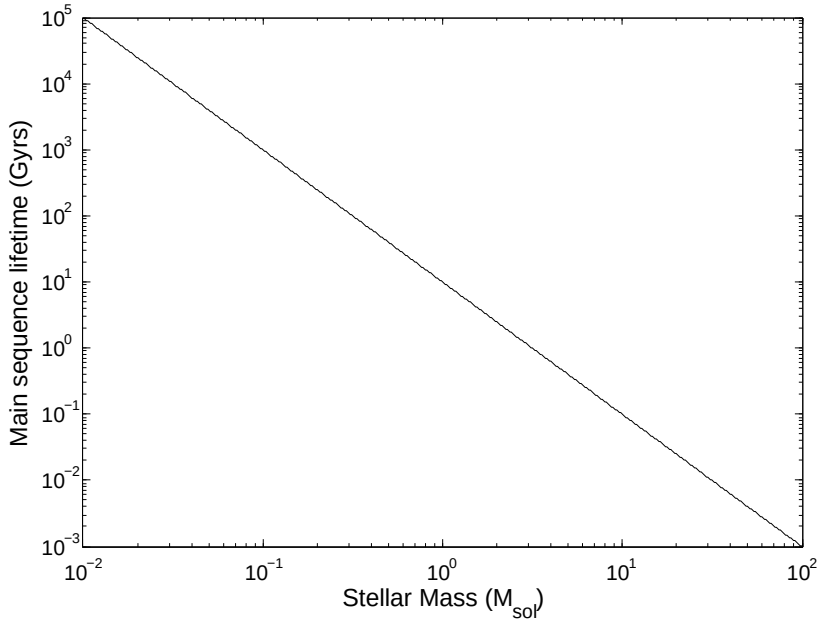

Figure 8: Log-log plot of stellar mass in $M_\odot$ against the main sequence (MS) lifetime in GYrs. The power-law of Equation 8 is clearly depicted.

As stars move away from the main sequence they'll eventually end up as remnants. These are listed in Table 3 along with the stellar masses that causes them.

Remnant	Mass ($M_\odot$)	Caused by ($M_\odot$)
White Dwarf	~ 0.6	$m < 8$
Neutron star	~ 1.4	$8 \leq m < 30$
Black hole	~ 10	$m \geq 30$

Table 3: Remnants and typical stellar masses that causes them. Black holes in this context are the stellar mass ones

4.1.4 Stellar metallicities

The stellar metallicity is a measure of how much helium and heavier elements a star contains. In this project the metallicity is referred to as the iron content of a star, [Fe/H].

$$[Fe/H] = \log(N_{Fe}/N_H) - \log(N_{Fe}/N_H)_\odot$$

N_X stands for the number of element X. The metallicity of a star is calculated relative the Sun as seen in the equation above, where the latter term is the value of metallicity for the Sun. When a star contains as much iron as the Sun, $[Fe/H] = 0$.

In our Galaxy there is a metallicity gradient (Pedicelli et al., 2009, Fig. 3 therein). This is a relation between radial distance from the galactic centre and the metallicity. With the knowledge that the massive objects acting as lenses are between us and the galactic centre, the metallicity according to the Pedicelli et al. (2009) will be in a range between 0 and +0.5 dex.

4.1.5 Planet population

From the same cloud of gas that forms the star, planets are formed. Intuitively, the higher the metallicity the more rocky materials to form planets. According to the core-accretion method of forming planets (Johnson, 2010, from now on JJ2010) there are three stages in planet formation. The early growth is in the μm domain and consists of sticking coagulation of particles. During mid-life growth bodies of ~ 10 km in size are made through gravitational attraction and are at the end of this stage, *cores*. In the late growth stage, the cores rapidly accrete gas and grow into sizes of $\sim 10^4$ km.

Higher mass or [Fe/H] means a faster core-production and thus more time for rapid gas accretion. This is favourable since stellar radiation and accretion onto the host star decreases the amount of surrounding gas in the cloud over time. The probability of harbouring a giant planet increases with stellar mass, but drops at $M > 3$ (Kennedy & Kenyon, 2008, Fig. 7 therein - from now on KK2007), because at larger stellar masses the lifetime of the disc becomes comparable with the time it takes to form the host star. When the

star is formed the disc begins to heat up, expand and thus dissipate. From KK2007

$$P_p = (0.2M_\star - 0.06)\alpha \tag{9}$$

where α is a normalisation constant chosen so that it fits with Udry et al. (2007) calculated value for solar properties. They state that 6,6% of the stars have giant planets (from RV surveys).

$$\begin{aligned} &P_p(1\ M_\odot) = 0.066 \\ &\Rightarrow P_p(m) = (0.2\frac{m}{M_\odot} - 0.06)\frac{1}{0.14} \end{aligned}$$

There is however another suggested relation from JJ2010 that states

$$P_p(m) \propto \left(\frac{m}{M_\odot}\right)^{1.13}$$

I chose to follow KK2007's linear relation, since $P_p(0.3\ M_\odot) = 0$ compared to the power-law form suggested by JJ2010 which has a $P_p(0.3\ M_\odot) \approx 0.26$. My guess is that the odds of a low mass star having a planet should be closer to 0 than what JJ2010 predicts.

The probability of harbouring giant planets as a function of metallicity (JJ2010) derived from RV survey data, is given by

$$P_p(F) = 0.066 \cdot 10^{1.07F} \tag{10}$$

where F is the metallicity [Fe/H]. So now the total probability of a star harboring a giant planet becomes

$$P_p(M, F) = 0.066 \cdot 10^{1.07F} \cdot \frac{1}{0.14}(0.2M - 0.06) \tag{11}$$

4.1.6 Planetary mass distribution

The planets themselves are also believed to follow a mass distribution similarly to how stars follow the IMF. Marcy et al. (2005) show that the distribution of exoplanets follow a power-law

$$\frac{dN}{dM_p} \propto (M_p \sin i)^{-1.05} \tag{12}$$

The data used to acquire the above relation is from RV surveys and as a result from that, the information regarding the inclination of the exoplanet orbit around its host star, is degenerate. Hence what's measured is really a minimum mass $M_{min} = M_{true} \sin i$, where i is the inclination of the orbit and can be anything between face-on (0°) to an edge-on (90°) orbit. Given

that the distribution of the inclination is uniform between these, the mean value becomes

$$\begin{aligned} y &= \sin i \\ i &= [0\ \pi/2] \\ \Rightarrow \bar{y} &= 2/\pi \end{aligned}$$

Equation 12 now becomes

$$\frac{dN}{dM_p} \propto (2/\pi)^{-1.05} \cdot M_p^{-1.05}$$

The method used to create the populations (explained in the next subsection) isn't in need of a normalisation and since the distribution of inclinations is uniform, the constant factor from the relation above can be removed.

$$\frac{dN}{dM_p} \propto M_p^{-1.05} \tag{13}$$

The relation is taken to be valid within the limits of $0.5\ M_{ju} \leq M_p \leq 15\ M_{ju}$.

4.2 The program

So how do we create the population of stars and planets? Using `MATLAB`, my goal in Stage One is to create an array of masses that should follow the IMF, array of metallicities (metallicity distribution) and array of ages (following the SFR). This is done with the use of a Monte Carlo (MC) method. Monte Carlo utilises random variables and probability statistics to investigate problems. The method used here is popularly called the "hit or miss" method. In the case of the mass distribution, we begin by encasing our function. This is easily imagined if one thinks of Figure 7 (IMF plot) being encased by a geometric shape that covers the entire area of interest. Random values are picked within that encasement.

$$\begin{aligned} m_{min} < m_{rand} < m_{max} \\ \xi_{min} < \xi_{rand} < \xi_{max} \end{aligned}$$

ξ_{rand} and m_{rand} are coupled. By making sure

$$\xi_{rand} \leq \xi(m_{rand}) \tag{14}$$

I ensure that the functional value always is "below" or equal to the function, these are hits and are saved in the array. The values that are "above" the function are branded as misses and are not saved. When this process has been repeated (iterations) N times, the array has now a certain length (#hits) that corresponds to:

$$\frac{\#hits}{N} = \frac{A_{below func.}}{A_{encasement}} \tag{15}$$

From Equation 15 one can easily calculate the integral of the function $A_{belowfunc.}$, which is what this MC method is commonly used for. In this project however, the integral was only calculated for the values in Table 2. The only information kept from this process is the mass, because of the distribution still being contained in the array (making a histogram of the masses would retrieve the shape of the function).

Similarly the metallicity and age was determined. Since I chose uniform distributions for these, we skip the restriction process (Similar to Equation 14) and just randomly generate values within a given interval. Stellar ages where picked from 0 to the Hubble time and metallicity between 0 and +0.5 dex. Each object has by now a mass, metallicity and age coupled to it, defined by three arrays in total.

The next step is what makes the PDMF. From Equation 8 (MS lifetime):

$$\tau_{rand} \leq \tau(m_{rand})$$

I'm making sure that if their ages are higher than their MS lifetime permits, they aren't main-sequence anymore, have evolved (become red giant and so forth) and become remnants according to Table 3. This is a valid assumption to make because of the short times spent by the stars on the post-Main sequence stages. After this, the PDMF has been created with $N_\star$ number of stars each with it's own mass, age and metallicity. From these, the planetary population is created.

A restriction similar to the ones put before is used when creating the planetary population, but with the functional value now determined by Equation 11 (Probability of forming a planet). Using the generated stellar mass, metallicities and a randomised functional value ($P_{p\ rand}$), a population of stars with planets is created. Like the IMF these planets have masses, with the use of Equation 13 and the same technique as before, the planetary masses are distributed.

Summarising Stage One, I created a number of stars $N_\star$ characterised by three arrays: mass, metallicity and age. Two of these arrays (mass and metallicity) were then used to create the planetary population. Lastly, an array was created for the planetary masses to be distributed, according to Equation 13.

4.3 Stage Two

The rate of μL events is determined by the probability for an event occurring with us as observers. One way of approaching it is to imagine the Einstein ring of a lens travelling across the sky, creating a band. (Figure 9).

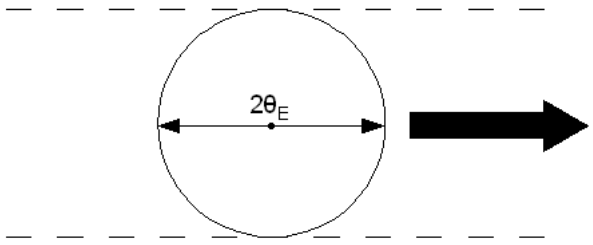

Figure 9: Schematic diagram of a lens and its Einstein ring. The lens draws a band as it moves on the sky

Larger lens mass means a larger θ_E and thus a wider band. The probability of a source star being located within this band, causing a μL event is subsequently then correlated with the lens mass.

$$\theta_E \propto m_L^{1/2} \tag{16}$$

$$rel.\ rate \propto m^{1/2} \tag{17}$$

As we pointed out before we aren't interested in the exact number of events, but the relative number of events. So the use of the proportionality (without any constants) is sufficient. In order to easily handle the data, the entire examined mass range (planetary masses + stellar masses) was divided into log-histograms, each with $N_{\star,i}$ stars and $N_{p,i}$ planets in the i:th bin and a mean mass

$$< m_i >= \frac{\sum_{j=1} m(j)}{N_{\star,i} + N_{p,i}}$$

Since planetary and stellar masses never overlap, when handling planetary masses (in the low part of the mass range) the stellar part $N_{\star,i}$ of the above equation is equal to 0. Correspondingly, when moving to stellar masses, the planets don't contribute to the mean mass. The reason for the use of log-histogram is because the entire mass range examined, planetary and stellar mass combined, stretches many orders of magnitude. That makes it easier to handle the data in log-space.

The relative rate, now with the use of log-histograms, becomes:

$$\Gamma_i = (N_{\star,i} + N_{p,i}) \cdot \sqrt{< m_i >} \tag{18}$$

In the same way, the average Einstein-time for each bin:

$$t_{E,i} \approx 25\ d\ \left(\frac{< m_i >}{0.5\ M_\odot}\right)^{1/2}$$

Summarising Stage Two, the star- and planet-populations where binned up into logarithmic histograms with the i:th bin having a mean mass of $< m_i >$, $N_{\star,i}$ stars, $N_{p,i}$ planets, a duration of $t_{E,i}$ and a relative event rate Γ_i.

4.4 Stage Three

Detectors rarely have a uniform detection. That is, they seldom have equal chance of detecting two objects that are at different sides of the spectrum. In μL surveys the signals at low masses are briefer (Equation 5) and therefore the resolution in time for an instrument restricts it. Having uniform detection will not change the relative distribution of the detected objects. In other words, it won't change the "shape" of the curve, only the scaling. This is important to remember since we're only interested in the relative distribution of detected FFPs to stars and not any exact numbers.

The Microlensing Observations in Astrophysics (MOA)[2] carried out a μL survey during 2000 with a non-uniform detection probability (Sumi et al., 2003, Fig.18 therein). A fit was extracted from their detection curve representing the detector efficiency of all possible source stars (Equation 19, Figure 10).

$$\ln \varepsilon = -6.44 + 1.01 \ln(t_E/d) - 0.15[\ln(t_E/d)]^2 \tag{19}$$

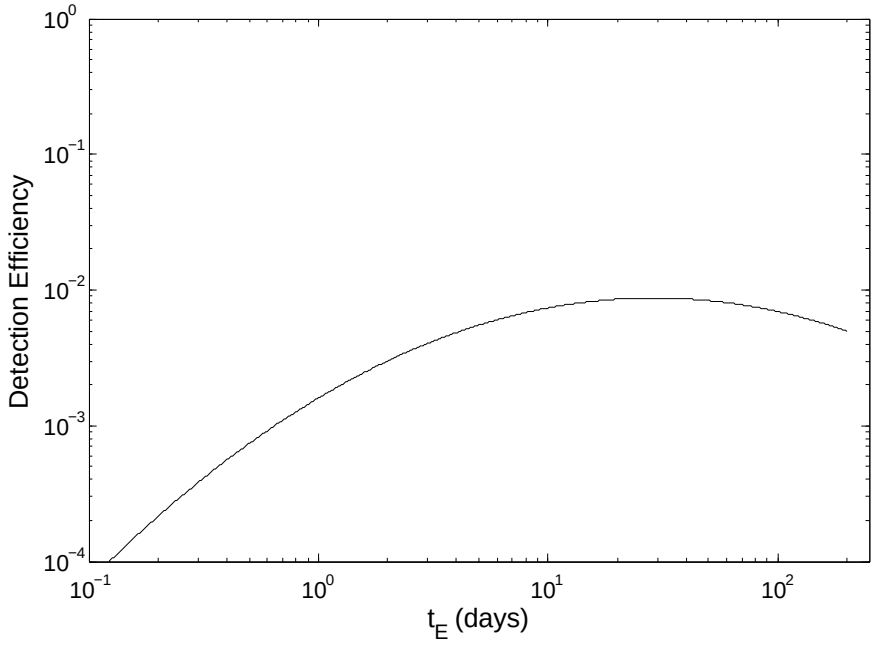

Figure 10: MOA detection efficiency for the ngb1–2 subfield for all source stars against t_E from Sumi et al. (2003) using an extracted fit (Equation 19). Low mass objects (for instance FFPs) are only detectable via μL through high magnification events (excellent alignment) which has a smaller probability of occuring.

[2]MOA homepage: `http://www.phys.canterbury.ac.nz/moa/`

The number of detected planets and stars is then a combination of Equation 19 and Equation 18:

$$\Upsilon(t_E) = \Gamma(t_E) \cdot \varepsilon(t_E) \tag{20}$$

For every bin, a value of $\Upsilon_i(t_{E,i})$ will be calculated. When plotting Υ against t_E the result will be similar to (Sumi et al., 2003, Fig.28). My own version of the plot is created for comparison using the Kroupa (2001) IMF, see Figure 11.

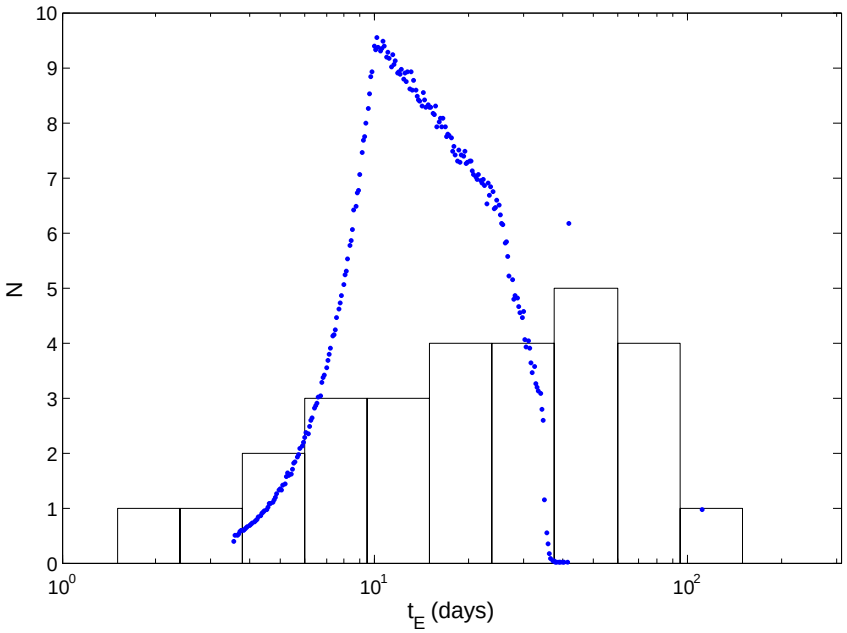

Figure 11: A plot displaying event duration t_E versus the number detected. The figure is adapted from Fig. 28 in Sumi et al. (2003) where the histogram displays the distribution for 28 observed events from the MOA survey whereas the curve is a theoretical prediction, using the PDMF, relative event rate and MOA detection efficiency from this paper. The power-laws inherited from the IMF are visible compared to the figure in Sumi et al. (2003) due to that there is no Galactic model taken into account in my theoretical prediction. What a Galactic model would do is mainly specify where in the galaxy our lenses are. Since the event duration t_E depends on the position of the lens (for same proper motions), the inclusion of such a model would "smoothen" out the curve of the theoretical prediction.

Figure 11 is a semi-log plot of the number of detected stars versus t_E. The curve represents the theoretical prediction of the stars whereas the histogram is observational data from 28 events (Sumi et al., 2003). As mentioned, Figure 11 only takes stellar objects into account. The lack of log-scale on the y-axis doesn't allow for planetary time-scales to be visible on the plot. In this paper I treat both planets and stars so instead of only having a peak

caused by stars, there will be an additional peak caused by the free floating planet population much like (Kamiya et al., in prep.) presents (Figure 12).

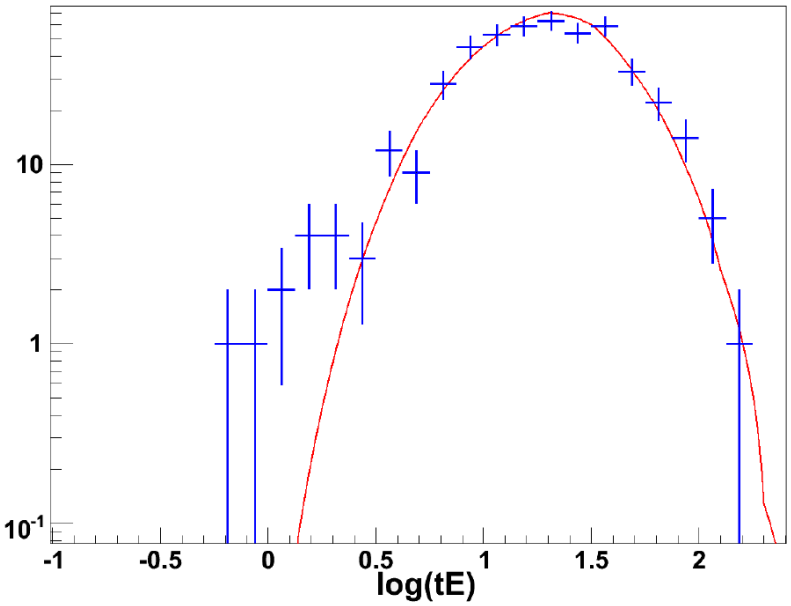

Figure 12: (Kamiya et al., in prep.) A collection of 2006-2007 data from the MOA collaboration. The line is a theoretical distribution from stellar population with a galactic model taken into account whereas the crosses are observational data. There seems to be an excess of short events that might be caused by free floating planets.

Additionally one must mention again that there won't be any effort put into getting the normalisations of all the parameters used to acquire the result, therefore the number of detections will instead be the relative number of detections.
Summarising Stage Three, for every bin the relative detected events $\Upsilon_i(t_{E,i})$ is calculated. The result is then presented by plotting $\Upsilon(t_E)$ against t_E.

5 Results

5.1 First run

5.1.1 Stage One

I assume for every star with planet, 1 planet has been ejected.

$$\therefore N_{\star\ w.planets} = N_{FFp}$$

The outcome of Stage One was $N_\star = 1,000,000$ and $N_{\star\ w.p} = N_{FFp} \approx 7000$
All the processes in this stage are manifested in Figure 13 through Figure 17.

Beginning with Figure 13, a uniform distribution of stellar ages was chosen which is easily noted in the figure.

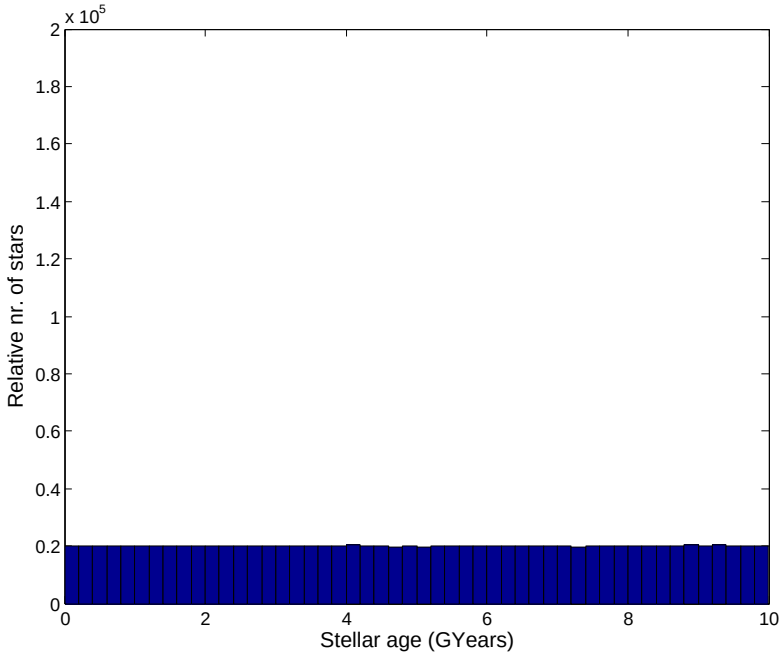

Figure 13: Histogram showing the relative distribution of stellar ages in the PDMF. The stellar ages are uniformly distributed because of the chosen uniform SFR.

From Figure 14 one can depict the logarithmic behaviour inherited from the IMF on the x-axis and the uniformly distributed stellar ages on the y-axis. To be clear, each point in the figure represents a stellar object. The curve cutoff at high masses is the MS lifetime restriction that doesn't allow for old heavy stars to exist as MS stars. Additionally, the three lines with higher density of points are the remnants (see Table 3).

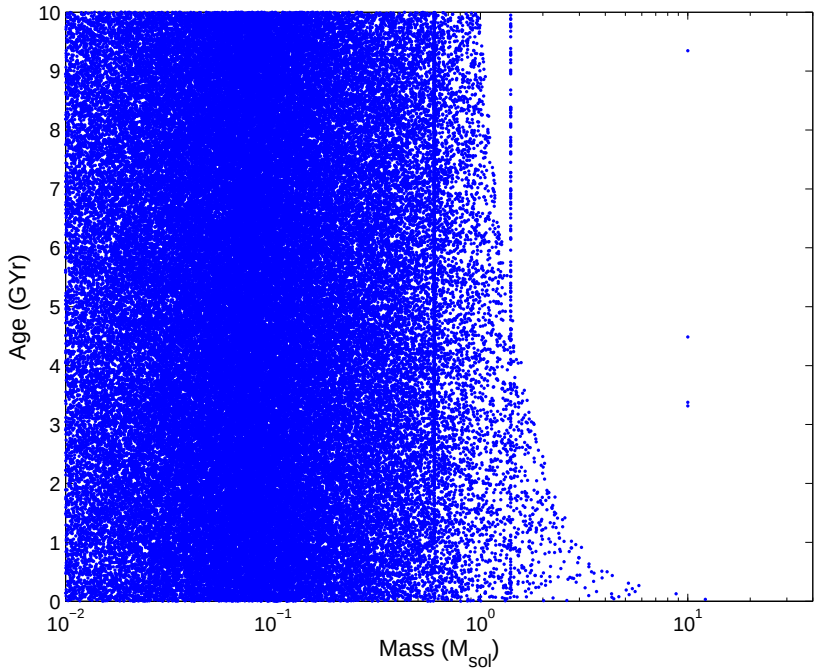

Figure 14: Logarithmic plot of the present-day population of stars showing their mass in $M_\odot$ against their age in years. The slope noticeable at higher masses is due to the MS lifetime restriction and the density shifts of the points follow the IMF.

When examining metallicity vs. mass for the stellar objects (Figure 15), the mass distribution is noticed, as before, along the x-axis aswell as the uniformity of the metallicity.

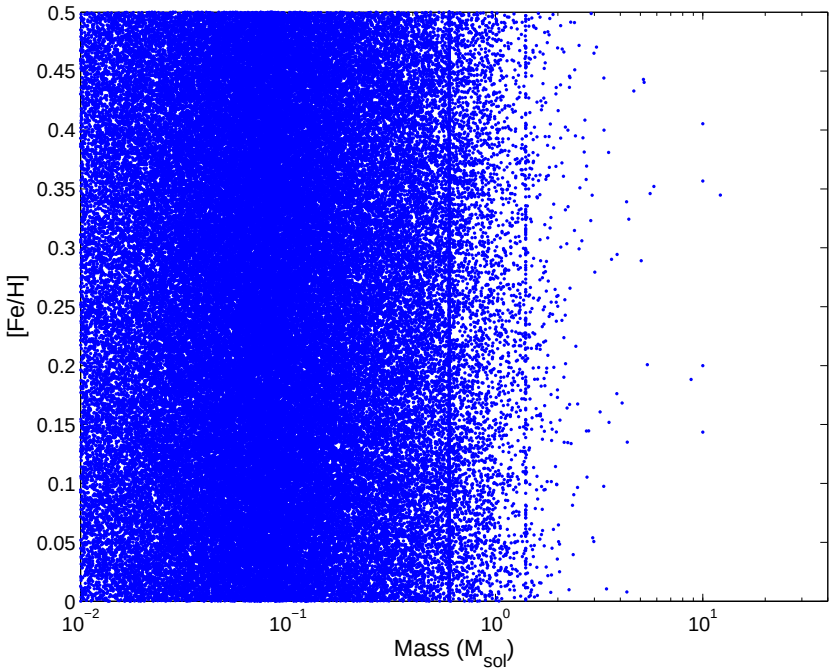

Figure 15: Logarithmic plot of the present-day population of stars. The stellar mass presented in logarithmic scale follows the IMF and is manifested by the density shifts of the points. The uniformity of metallicity is also clearly displayed.

Heavier and more metal rich stars are favoured in the process to have planets (Johnson, 2010). Figure 16 displays the population of stars with planets (created using Equation 11) and how they fit in a Mass versus Metallicity plot. The cutoff at lower masses comes from the use of KK2007 that causes the probability to be zero at stellar masses of $\simeq 0.3\ M_{\odot}$.

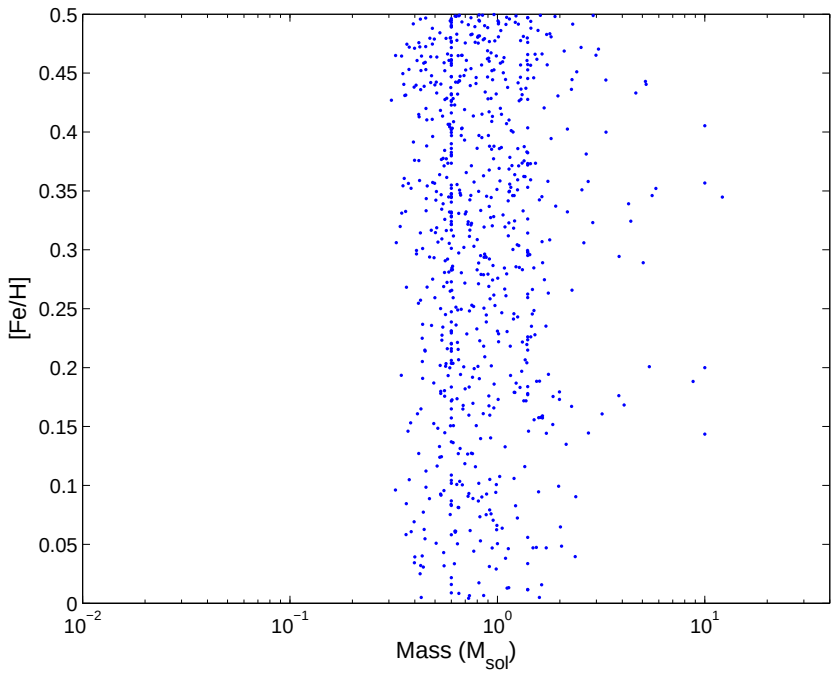

Figure 16: Logarithmic plot displaying the population of stars harboring planets. Stars with higher metallicities are favoured when creating planets which is manifested in this plot by the higher density of points at higher metallicities. The same goes with stellar mass with the addition of a low cutoff at a stellar mass of $\simeq 0.3\ M_{\odot}$

Since a potential correlation between planet creation and stellar age is neglected, the plots showing the masses of the population of stars with planets plotted against their age, will be similar to the one containing all stars (PDMF) except for the cutoff introduced from KK2007.

The mass distribution of the planets where chosen to follow the power-law presented earlier (Marcy et al., 2005). Seen in Figure 17, the distribution follows the trend given by the power-law within the limits put at 0.5 and 15 M_{ju}. The free floating planets are then assumed to follow the same distribution.

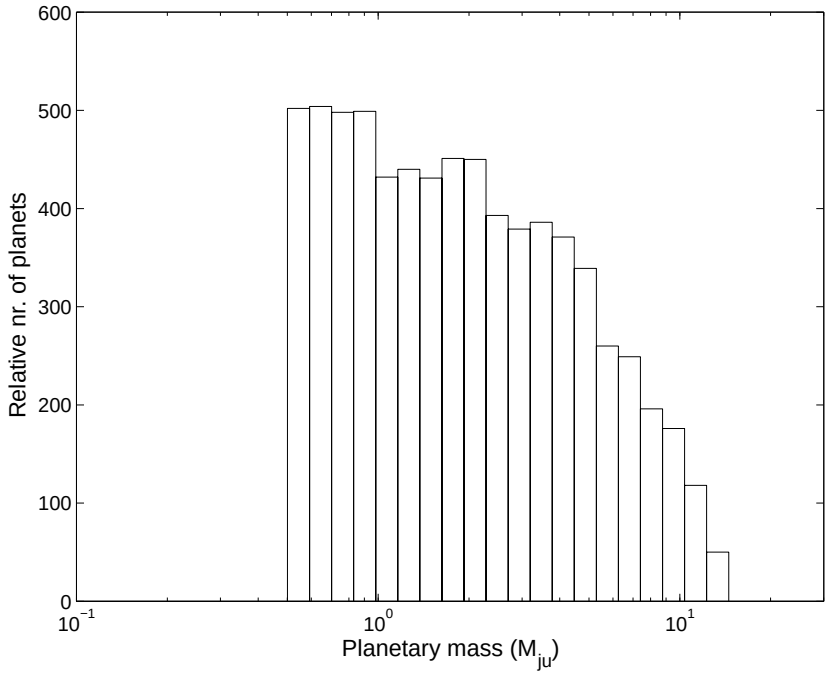

Figure 17: The planetary mass distribution of observed exoplanets using the single power-law of Equation 13 radial velocity measurements from Marcy et al. (2005). The drastic drop at low masses is a limit set at 0.5 M_{ju} in order to prevent the function to otherwise explode when moving towards 0 M_{ju} and thus not astrophysically motivated. An upper limit of 15 M_{ju} was also set. The free floating planets are assumed to follow the same mass distribution.

5.1.2 Stage Two & Three

In order to acquire a Kamiya et al.-like plot, the relative rate of events (Stage Two) is multiplied with detector efficiency fit Figure 10 (Stage Three, MOA detection efficiency plot), which yields Figure 18.

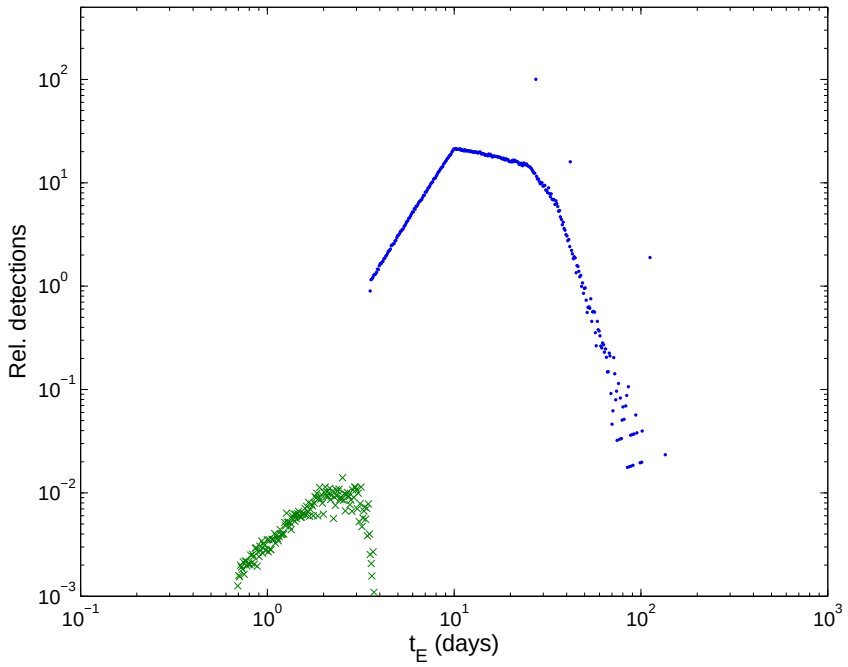

Figure 18: Kamiya et al. like plot using the Kroupa (2001) stellar mass distribution, a uniform star formation rate and metallicity range, a simple equation for the MS lifetime and the Marcy et al. (2005) planetary mass distribution. As explained earlier, the differences in shape (when comparing to Kamiya et al. (in prep)) of the lines arise from the fact that no Galactic model was used in my model. Inclusion of that would smoothen out the shape. The three points/bars standing out of the curve at durations of roughly 30, 40 and 100 days are the three different compact remnants (white dwarf, neutron stars and black holes respectively) caused by stellar evolution.

By taking the area below the detected stars ($Det_\star$) and dividing with the area below the detected free floating planets (Det_{FFP}) in Figure 18, one answers the main question: "How many stellar μL-events does one need to see before one expects to see one that is caused by a FFP?"

$$\frac{Det_\star}{Det_{FFP}} = \frac{\sum_i h_{\star,i} w_{\star,i}}{\sum_i h_{FFP,i} w_{FFP,i}}$$

where h is the height of the peak and w is the width of the bin. Since the width didn't change in log space with bin number and object type (planet

or star), the above equation is simplified to

$$\frac{Det_\star}{Det_{FFP}} = \frac{\sum_i h_{\star,i}}{\sum_i h_{FFP,i}} \simeq 3.0 \cdot 10^3 \ stars$$

Comparing the relative height between the peak caused by stars and planets from the observational data (Figure 12) and the plot generated from the first run (Figure 18), the later has a higher difference, so the $Det_\star/Det_FFP$ from the MOA observational data are many orders of magnitude lower, i.e there are more low-duration objects detected per detected star in the observational data. This might be due to uncertainties in the assumptions used for calculating Figure 18.

5.2 Uncertainties

Figure 18 was generated by a program with editing capabilities. Stellar and planet attributes can easily be altered in order to see how much impact they will have on the result. The following attributes were altered

5.2.1 Stellar metallicity

The metallicity range was altered between the previous uniform distribution (between 0 and +0.5 dex), to all being solar-like (0).

5.2.2 Star formation Rate

The SFR history being formerly uniform could be exponentially declining with time simulating an explosion in stellar creation at the beginning of time.

$$SFR = \frac{dN}{dt} \propto e^{-t/T} \tag{21}$$

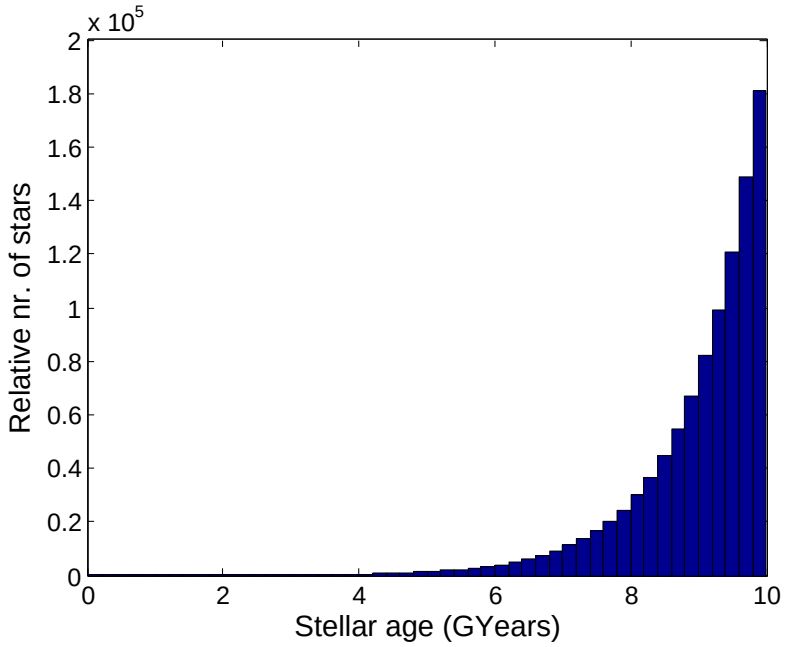

Figure 19: Histogram showing the relative distribution of stellar ages in the PDMF. Since this SFR assigns generally higher ages, there'll be less number of older stars left in present time compared to when one uses the uniform SFR.

where T was set to 1 Gyr. Displayed in Figure 19 is a histogram of the stellar object's age distribution using the above relation for the SFR. This is to be compared with the uniform distribution of ages shown in Figure 13. As an effect of the Non-uniform SFR assigning higher ages, there will be a less number of older stars when comparing to the uniform SFR due to their short MS lifetimes.

5.2.3 Main sequence lifetime

The uncertainty in the Main sequence lifetime calculation was checked with a more advanced formula. Eggleton et al. (1989) presents the following formula for calculating the MS lifetimes.

$$\tau_{MS} = \frac{2550 + 669M^{2.5} + M^{4.5}}{0.0327M^{1.5} + 0.346M^{4.5}} \; Myr$$

A comparison of the two MS lifetime formulae is seen in Figure 20.

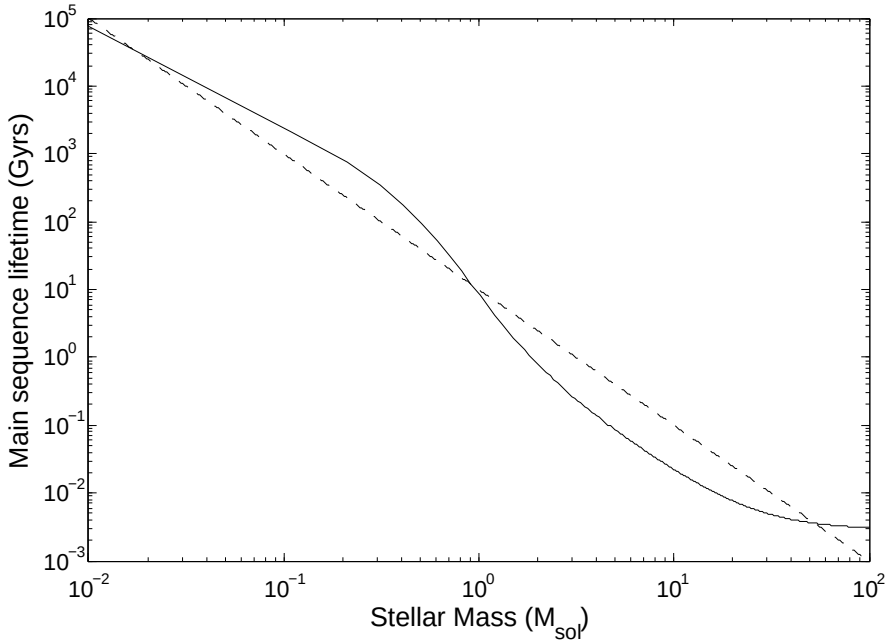

Figure 20: Log-log plot of stellar mass in $M_{\odot}$ against MS lifetimes in GYears using the more advanced formula (Eggleton et al., 1989) in continuous line, to be compared with the simpler single power-law relation from Marcy et al. (2005) (Figure 8) in dashed line.

5.2.4 Planet mass distribution

The planetary mass distribution of Marcy et al. (2005) was checked against one presented in Mordasini et al. (2009). Seen in Figure 21 the alternative distribution covers a larger span of planetary masses and can populate the low mass end since it doesn't explode when moving towards 0 M_{ju}. It is therefore in no need of a low mass limit as the previous planetary mass distribution did.

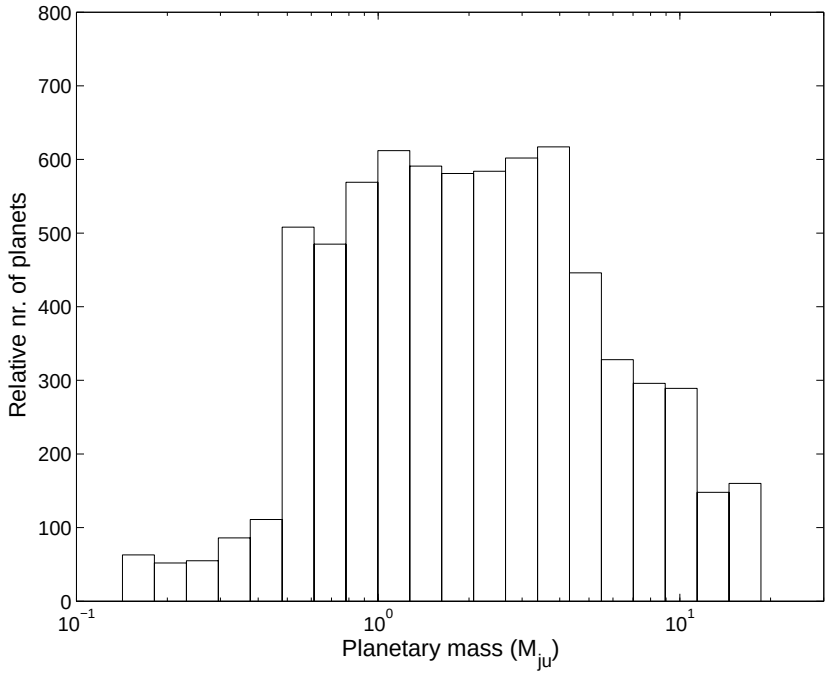

Figure 21: Adapted version of the planetary mass distribution presented in Mordasini et al. (2009) to be compared with the single power-law distribution from Marcy et al. (2005). Unlike the previous distribution, no limits has to be set which allows for low planetary masses.

For the above mentioned alterations, simulations can be run with all the permutations (which adds up to a total of 16 simulations). The answer to the main question in this project, i.e "How many stellar μL-events does one need to see before one expects seeing one that is caused by a FFp?" is answered for each combination and presented in Table 4, including the first run.

Z	SFR	MS	M_p	N_{FFP}	Detected $\frac{N_\star}{N_{FFP}}$ $(/10^3)$
1	1	1	1	5600	3.2
1	1	1	0	5700	3.7
1	1	0	1	6000	3.1
1	1	0	0	5900	3.5
1	0	1	1	6400	2.9
1	0	1	0	6400	3.3
1	0	0	1	7200	2.6
1	0	0	0	7100	3.0
0	1	1	1	2900	6.6
0	1	1	0	2900	7.2
0	1	0	1	2900	6.2
0	1	0	0	3000	6.8
0	0	1	1	3200	5.9
0	0	1	0	3200	6.5
0	0	0	1	3700	4.9
0	0	0	0	3700	5.7

Table 4: All the configurations from the listed variations.
Z marks whether the metallicity is solar like for all (0) or uniform between 0 to +0.5 dex (1)
SFR is either uniform (0) or exponentially declining with age (1)
MS (Main sequence lifetime) is either determined with a simple relation (0) or more complex (1)
M_p distribution is either determined by the power-law from Marcy et al. 2005 (0) or Mordasini et al. 2009 (1).
The final column displays how many stars that are detected per detected free floating planet rounded to one decimal and is the answer to the main question in this project. $N_\star = 1,000,000$ in all simulations. The first run had a configuration of 1,0,0,0

For comparison, a plot similar to that of Figure 18 was generated but using the opposite configurations (Figure 22). That is: All stellar metallicities being solar, exponentially declining stellar age distribution (more older stars), more complex MS lifetime calculation and Mordasini et al. (2009) planetary mass distribution.

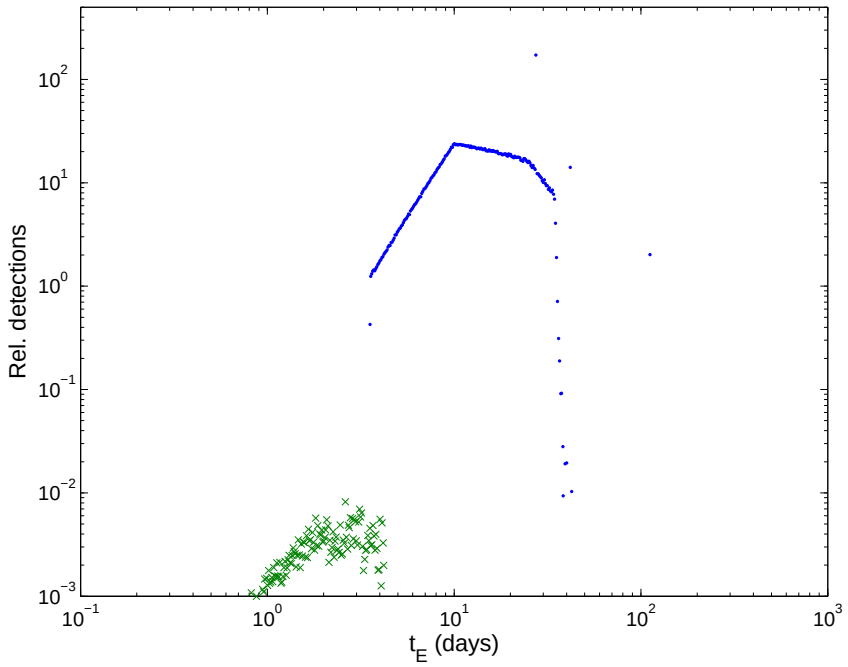

Figure 22: This figure shows the event duration versus relative number of detections. It's generated using different assumptions compared to the first run (Figure 18). Specifically, this figure was generated with the following attributes: All stellar metallicities being solar, exponentially declining stellar age distribution (more older stars), more complex MS lifetime calculation and Mordasini et al. (2009) planet mass distribution. When comparing to the first run, there are more points for the planetary peak at lower durations because the planetary mass distribution used allows for low mass planets to exist. Again the three points/bars at durations of roughly 30, 40 and 100 days are the three types of remnants (white dwarfs, neutron stars and black holes) resulted from stellar evolution. Also, the decrease in points at high durations is a consequence of the exponentially declining SFR. Generally higher stellar age means generally less remaining stars, especially at higher stellar masses

From Table 4, one can see that Detected $\frac{N_\star}{N_{FFP}}$ varies at about a factor 2 between the different combinations. So the uncertainty would be at about this level. However, this level of uncertainty still doesn't account for the difference seen between Figure 18 (first run) and Figure 12 (MOA Observational data).

6 Discussion

The height of the planetary or stellar peaks are only dependent on how many objects (planets or stellar objects respectively) there are. In order to reach the same relative difference, the planetary peak of the first run must be increased by a factor of ≈ 470 resulting in the following populations.

$$N_\star = 1,000,000$$
$$N_{FFP} \approx 3,400,000$$

$$\Rightarrow \frac{N_{FFP}}{N_\star} \simeq 3.4 \ (3)$$
$$Detected \frac{N_\star}{N_{FFP}} \simeq 6.2 \ (6)$$

The parentheses in the end are to emphasise that one cannot have non-integer number of objects. The calculated number of free-floating planets per star ($\frac{N_{FFP}}{N_\star}$) is equal to the one presented in Gaudi (2010b) for the observational data. This was by assuming that the observational data (Figure 12) is unbiased, has enough number of observations to avoid large uncertainties due to standard deviations and that all short-timescale events are caused by free-floating planets. The fact that the two values are equal validates the program used in this project. Using this data and the MOA detection efficiency, I get that one detects approximately 6 stars before one expects to detect a free floating planet.

The plausibility of this, is in my opinion, doubtful since it would mean 470 free-floating planets per star with planets (first run was 1 free-floating planet per star with planets). It is however not clear whether the short-duration peak in the observational data was only due to FFPs, as planets in very wide orbits (similar to those that have been imaged directly orbits of $\sim 100s$ AU) may also add to these (Gaudi, 2010b) and cause the increased height in the planetary peak. Another possible explanation is that there might be a larger percentage of stars that have planets than what is known. A higher fraction of extrasolar systems means more FFPs which would up the planetary peak.

The knowledge of the free floating planet population is crucial to our understanding of planetary creation processes and the stability of planetary systems. A number of questions that can be answered are for instance the frequency of FFPs (as discussed previously), how usual is planet ejection? With knowledge of their masses: How does their masses distribute?, Does it differ with other planetary distributions, and if so, why? There are two competing theories for planet creation, one being the core accretion method mentioned in this report. The other one is called gravitational instability.

The latter one predicts production of planets at large orbits. These have higher tendencies of being pulled away, making them free floating planets by passing stars, as opposed to the more close-bound planets predicted by core-accretion. If the observed free floating planetary mass distribution is heavier than suspected from core accretion, then it might be an observational proof of this.

Using a similar program as the one created for this project and better observational data that'll come out of future surveys, one can work out what the free floating planet mass distribution is but also verify the stellar mass function. Additionally, knowing how many free floating planets that exist out there, might put a restriction on the fraction of extrasolar systems compared to stars.

7 Acknowledgements

First off I'd like to thank my supervisors Melvyn B. Davies and Ross Church for being very helpful throughout the project and also for helping me out grammatically. I'd also like to thank Nils, Tobias, Hannes and Fredrik for being excellent neighbours and wish them luck on their future Ph.D projects. Finally, I'd like to thank my roommate Kalle for putting up with me on all the long discussions and countless monologs but also Emma who helped out with some corrections.

References

Beatty, J. K. & Chaikin, A. 1990, The New solar system / edited by J. Kelly Beatty, Andrew Chaikin ; introduction by Carl Sagan, 3rd edn. (Cambridge University Press ; Sky Pub. Corp., Cambridge [England] ; New York : Cambridge, Mass. :), viii, 326 p. :

Eggleton, P. P., Tout, C. A., & Fitchett, M. J. 1989, ApJ, 347, 998

Einstein, A. 1936, Science, 84, 506

Gaudi, B. S. 2010a, ArXiv e-prints

Gaudi, B. S. 2010b, kITP Conference: Exoplanets Rising: Astronomy and Planetary Science at the Crossroads, `http://online.itp.ucsb.edu/online/exoplanets_c10/gaudi/`

Gould, A. 2001, in Astronomical Society of the Pacific Conference Series, Vol. 239, Microlensing 2000: A New Era of Microlensing Astrophysics, ed. J. W. Menzies & P. D. Sackett, 3–+

Johnson, J. 2010, kITP Conference: Exoplanets Rising: Astronomy and Planetary Science at the Crossroads, `http://online.itp.ucsb.edu/online/exoplanets_c10/gaudi/`

Kamiya et al. in prep., MOA Observational data 2006-2007

Kennedy, G. M. & Kenyon, S. J. 2008, ApJ, 673, 502

Kroupa, P. 2001, MNRAS, 322, 231

Malmberg, D. & Davies, M. B. 2009, MNRAS, 394, L26

Marcy, G., Butler, R. P., Fischer, D., et al. 2005, Progress of Theoretical Physics Supplement, 158, 24

Mordasini, C., Alibert, Y., Benz, W., & Naef, D. 2009, A&A, 501, 1161

Pedicelli, S., Bono, G., Lemasle, B., et al. 2009, A&A, 504, 81

Sumi, T., Abe, F., Bond, I. A., et al. 2003, ApJ, 591, 204

Udry, S., Fischer, D., & Queloz, D. 2007, Protostars and Planets V, 685

Wright, J. T., Upadhyay, S., Marcy, G. W., et al. 2009, ApJ, 693, 1084